

# Lab on a Chip

Accepted Manuscript



This is an *Accepted Manuscript*, which has been through the Royal Society of Chemistry peer review process and has been accepted for publication.

*Accepted Manuscripts* are published online shortly after acceptance, before technical editing, formatting and proof reading. Using this free service, authors can make their results available to the community, in citable form, before we publish the edited article. We will replace this *Accepted Manuscript* with the edited and formatted *Advance Article* as soon as it is available.

You can find more information about *Accepted Manuscripts* in the [Information for Authors](#).

Please note that technical editing may introduce minor changes to the text and/or graphics, which may alter content. The journal's standard [Terms & Conditions](#) and the [Ethical guidelines](#) still apply. In no event shall the Royal Society of Chemistry be held responsible for any errors or omissions in this *Accepted Manuscript* or any consequences arising from the use of any information it contains.

## PAPER

Cite this DOI:  
10.1039/x0xx00000x

## Toward instrument-free digital measurements: a three-dimensional microfluidic device fabricated in a single sheet of paper by double-sided printing and lamination†

Seong-Geun Jeong,<sup>a</sup> Sang-Ho Lee,<sup>b</sup> Chang-Hyung Choi,<sup>a</sup> Jiyun Kim<sup>a</sup>  
and Chang-Soo Lee\*<sup>a</sup>

This study demonstrates a simple approach for fabricating a 3D- $\mu$ PAD from a single sheet of paper by double-sided printing and lamination. First, a wax-printer prints vertically symmetrical and asymmetrical wax-patterns onto a double-sided paper surface. Then, a laminator melts the printed-wax-patterns to form microfluidic channels in a paper sheet. The vertically symmetrical wax-patterns form vertical channels when the melted wax-patterns make contact with each other. The asymmetrical wax-patterns form lateral and vertical channels at the cross-section of the paper when the printed-wax-patterns are melted to a lower height than the thickness of a single sheet of paper. Finally, the two types of wax-patterns form a 3D microfluidic network to move fluid laterally and vertically in a single sheet of paper. This method eliminates major technical hurdles related to the complicated and tedious alignment, assembly, bonding, and punching process. This 3D- $\mu$ PAD can be used in a multiplex digital assay to measure the concentration of a target analyte in a sample solution simply by counting the number of colored bars at a fixed time. It does not require any external instruments to perform the digital measurement. Therefore, we expect that this approach could be an instrument-free assay format for use in developing countries.

Received 00th January 2014,  
Accepted 00th January 2014

DOI: 10.1039/x0xx00000x

[www.rsc.org/](http://www.rsc.org/)

## PAPER

## Introduction

The increasing percentage of elderly patients with high risks of disease has led to an increase in the social cost of diagnosis.<sup>1,2</sup> Currently, the cost of diagnosis and treatment is a serious problem in the world.<sup>2</sup> In particular, the cost of personal diagnosis represents a significant burden in developing countries, where access to medical technology is limited. Although commercially available modern diagnostic systems provide sensitive and selective analysis, they are difficult to implement in resource-limited regions because they are expensive and large instruments, there are few well-trained experts, the infrastructure is poor, and they require large volumes of reagents.<sup>3</sup> The World Health Organization has clearly defined the criteria as a benchmark to decide if diagnostic tests address disease control needs: affordable, sensitive, specific, user-friendly, rapid and robust, equipment-free and deliverable to end-users.<sup>4</sup> In fact, “equipment-free” is one of seven necessary attributes for diagnostic tests in developing regions. Thus, the use of external readers and pumps must be overcome when creating ideal (POC) diagnostic tests for use in the developing world.<sup>5,6</sup>

Recently, microfluidic paper-based analytical devices ( $\mu$ PADs) have attracted considerable attention for use in a wide range of applications because they provide a portable, cheap, disposable, simple, and rapid assay that requires small volumes of sample and reagents.<sup>7-11</sup>  $\mu$ PADs can be classified into two categories, depending on the dimensions of the microfluidic channel. First, is a two-dimensional  $\mu$ PAD (2D- $\mu$ PAD), which is designed to laterally move fluid in the x-y plane.<sup>5, 9, 12, 13</sup> Second, is the three-dimensional  $\mu$ PAD (3D- $\mu$ PAD), which can flow in the z-direction and has been fabricated by stacking 2D- $\mu$ PADs.<sup>6, 14</sup> Fluid in a 3D- $\mu$ PAD can freely move in both the horizontal and vertical directions. Compared with 2D- $\mu$ PADs, 3D- $\mu$ PADs offer several advantages that cannot be achieved in a 2D- $\mu$ PAD, such as an increased number of assays on a small device, a rapid distribution of sample owing to the short moving distance in the vertical direction compared to the lateral direction, and the ability to perform multiple pre-processing or reaction steps.<sup>15-17</sup>

Although 3D- $\mu$ PADs have clear benefits for the rapidly growing field of paper-based microfluidic devices, there are some important drawbacks in the conventional fabrication techniques, such as the use of double-sided adhesive, origami-clamping, and the spray adhesive gluing method.<sup>6, 14, 17, 18</sup> These methods require more complicated fabrication processes than 2D- $\mu$ PADs to create more complex flow channels, including vertical channels that do not exist in 2D- $\mu$ PADs. To form a vertical flow channel, the original fabrication method involves the precise stacking and alignment of multiple sheets of paper, pasting with a double-sided adhesive, punching holes in the sheets, and the addressing holes with hydrophilic materials during assembly.<sup>6, 14</sup> Finally, fluid can flow vertically through adjacent paper layers. Especially, in the case of a hydrophobic double-sided adhesive tape, the holes should be made on the tape. The formation of a hole results in a gap or space between the two layers of papers. Thus, an additional process to fill the

holes with hydrophilic materials, such as cellulose powder, or to connect adjacent paper sheets through a compressive process is a prerequisite for flowing through the holes.<sup>6, 14</sup> In case of the spray adhesive gluing method, even though it can avoid the tedious alignment and assembly steps, the use of soluble adhesive in common solvents is likely to contaminate the sample or detection reagents. Therefore, the existing complicated fabrication process should be simplified and rapid to allow for commercialization of 3D- $\mu$ PADs and make them a more widely available tool as a zero-cost diagnostics.

Herein, we present a simple and rapid method for fabricating a 3D- $\mu$ PAD using double-side printing and lamination as an adhesive and alignment free process. The fabrication process involves two steps: (1) double-side printing of wax-patterns and (2) lamination for heating the wax-patterns. The lamination process rapidly melts the wax-patterns and forms a 3D-microfluidic network in a single sheet of paper. By manipulating the heating time and speed in the laminator controls, the width and height of the wax pattern on the paper can be controlled. Based on this approach, a paper device containing a 3D-microfluidic network on a single sheet of paper can be easily produced in a personal office or common laboratory without involving complicated instruments. This method minimizes the number of paper layers that need to be aligned and assembled. Additionally, this fabrication approach provides programmable fluid flow in a single sheet of paper so that digital diagnostic tests can be performed without the use of an external detection apparatus.

## Experimental

### Chemicals

All chemicals were obtained from Sigma-Aldrich (St. Louis, MO, USA) and were used without purification. Bovine serum albumin (BSA) and glucose were dissolved in distilled water at different concentrations to prepare sample solutions. We applied a dye-binding method for albumin in the sample that is based on tetrabromophenol blue (TBPB) (0.688 mg mL<sup>-1</sup> in 50% ethanol), a dye that has a reliable sensitivity and specificity for albumin. The detection of glucose was performed by consecutive reactions with potassium iodide and a mixture of glucose oxidase and horseradish peroxidase (5:1) (starch assay kit, Sigma-Aldrich).<sup>5, 19, 20</sup> The color changes from colorless to brown when potassium iodide binds to the hydrogen peroxide produced by the enzymatic reaction.

### Paper, printer, and laminator

Whatman® cellulose chromatography paper (Grade 3 MM Chr, Sigma-Aldrich, MO, USA) was used because it is hydrophilic, biocompatible, and reproducible. The average thickness of the paper used in this study (340  $\mu$ m) was sufficient to form a 3-dimensional microfluidic channel in a single sheet of paper. After lamination, the average thickness of the paper was decreased to 290  $\mu$ m due to the effects of pressing during the laminating process. We used a wax printer (Xerox ColorQube

8870, USA) because it was commercially designed to print solid wax. The printed wax-patterns form microchannels as they cool, and they solidify instantaneously without further spreading. A laminator (PhotoLami-350R6, Hyundai Office CO., LTD, Republic of Korea) was used for melting and spreading the printed wax-pattern because it was able to control the rate of laminating based on the rotation rate of two hot rollers. It also provided uniform heat-transfer while heating the paper for a few seconds. Two hot rollers transferred heat to the printed-wax-patterns on both-sides of the paper while it moved from the inlet to the outlet of the laminator. Simply, the rotation rate of the roller precisely controls the heated height of the wax-patterns in thin paper. Therefore, the height of the wax-patterns can be controlled by manipulating the rotation rate of the hot roller in the laminator.

### Formation of a microfluidic network in a single sheet of paper

We designed hydrophobic wax patterns using image software (Adobe Illustrator CS6) and printed the patterns on paper using a solid ink printer set to the parameters for photoquality printing. The primary fabrication procedure consisted of two steps, double-side printing and lamination (Fig. 1). First, the designed wax-patterns were printed on both sides of a sheet of paper (Fig. 1(A)). The printed paper was then heated by a laminator set at 140 °C for 0.26 sec, and the wax patterns were melted and spread through the thickness of the paper (Fig. 1(B)). The 3-dimensional microfluidic network containing an inlet or outlet and microchannels was formed in a single sheet of paper after removing the paper from the laminator and allowing it to cool to room temperature (< 20 sec). A detailed description of the experimental procedure and the basic design is included in Fig. S1, S2 in the ESI.†

### Fabrication of a $\mu$ PAD for detecting BSA and glucose

Furthermore, we expanded our approach to develop a novel equipment-free assay for straightforward and quantitative  $\mu$ PAD measurements. Feasibility was demonstrated by the quantitative detection of BSA and glucose as model analytes. The fabrication principle and process are schematically shown in Fig. 5 and Fig. S4.† The  $\mu$ PAD consisted of a sample pad, a glucose dot, and BSA dots. The glucose assay was performed by enzymatic oxidation of iodide to iodine, in which a color change from clear to brown is associated with the presence of glucose in the sample solution.<sup>5, 19</sup> Prior to the assay, the glucose dots were functionalized by the sequential absorption of a potassium iodide solution and an enzyme mixture containing horseradish peroxidase and glucose oxidase. For the protein assay, we have adopted the color change of TBPB when it ionizes and binds to albumin.<sup>21</sup> The presence of protein in a sample solution induces a color change from yellow to blue.<sup>22</sup> For the protein assay, we spotted 1.5  $\mu$ L of a 250 mM citrate buffer solution, and then layered TBPB solution (0.688 mg mL<sup>-1</sup>, 3  $\mu$ L) over the citrate buffer solution. The spotted reagents were allowed to air dry at room temperature. The final assembled  $\mu$ PAD was stored at 4 °C, which maintained the sensitivity after 7 days compared to day one.

### Image analysis

An optical microscope (Nikon SMZ800, Japan) equipped with a ccd camera (Phantom MIROEX2, USA) was used to capture

images of the melted wax in the cross-section of the paper. The images were analyzed using Image J software.

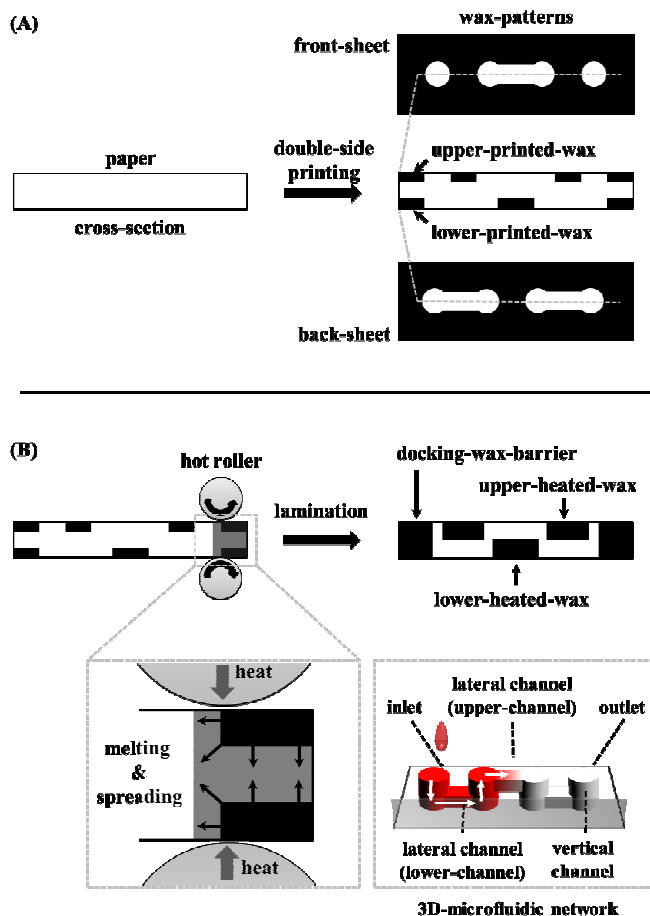


**Fig. 1** Schematic of the fabrication method for 3D paper-based microfluidic analytical devices (3D- $\mu$ PADs) based on double-sided printing and lamination. (A) Double-side printing: a wax printer prints the wax-patterns on the both-sides of a sheet of paper. (B) Lamination: two hot rollers in a laminator melt the wax-patterns, and the heating time can be controlled by adjusting the rotation rate of the hot rollers. A docking-wax-barrier, upper-heated-wax and lower heated-wax are formed with a proper heating-time (0.26 sec). A docking-wax-barrier is formed when the spreading upper-heated-wax contacts the lower-heated-wax. It functions as an inlet and outlet. Lower- and upper-channels are formed by the lower-heated-wax and the upper-heated-wax, respectively. Based on this approach, a 3D microfluidic network is formed in a single sheet of paper. The liquid (red dye solution) flows vertically and horizontally from inlet to outlet via lower-channels and an upper-channel.

## Results and discussion

### Formation of a 3D microfluidic channel in a single sheet of paper

In this study, a new printing approach is described for the formation of a 3D-microfluidic network using simple double-sided wax printing and thermal lamination to spread the printed wax (Fig. 1A). This method uses cheap and commercially available printer and laminator sold for stationary. This process minimizes the number of layers of material that need to be aligned and assembled (Fig. S5).† This approach also provides

way to program fluid flow within a single sheet of paper so that the results of a diagnostic assay can be displayed by the change of color of a reagent. This method involves two simple steps: double-sided printing and thermal lamination. The entire process can be completed in approximately in 35.5 sec (Table S1).<sup>†</sup> In this study, we have used wax printing because wax can be printed directly onto paper in well-defined patterns to create hydrophobic, impermeable barriers with well-controlled height that function as channels to wick the fluid. The 3D-microfluidic channel in a single sheet is obtained by precisely controlling the spreading of molten wax during the thermal laminating process (Fig. 1B). A docking-wax-barrier is formed when vertically symmetrical printed-wax-patterns are melted and contact each other after heating during lamination. This barrier plays a role as a hydrophobic barrier to prevent hydrophilic fluid from leaking in the paper. Then, upper- or lower-channels are formed when vertically asymmetrical printed-wax-patterns are melted and spread. The well-controlled thermal lamination produces independent lower- and upper-heated-wax patterns. Finally, these symmetrical and asymmetrical wax patterns develop microchannels to allow fluid to flow horizontally or vertically along upper- and lower-channels (Fig. 1B).

### Control of the heated height and width

The spreading of the printed wax pattern in the paper is a process of capillary flow in porous media that can be described by Washburn's equation (1).<sup>23</sup> This equation indicates that the spreading distance strongly depends on the viscosity of the molten wax, which is a function of the temperature.<sup>24</sup> Thus, a uniform heating process is prerequisite for the fabrication of a reliable microfluidic network in paper.

$$L^2 = \frac{\gamma Dt}{4\eta} \quad (1)$$

where  $L$  is the distance that a liquid of viscosity ( $\eta$ ) and surface tension ( $\gamma$ ) penetrates into a porous material with an average pore diameter ( $D$ ) over time ( $t$ ). The wax will spread laterally and vertically in the paper. The distance moved by the molten wax will be constant under well-controlled heating and pressure condition (Fig. 2A). Vertical spreading of a printed wax pattern creates hydrophobic barriers and controls the height of the channel, whereas lateral spreading between wax patterns produces channels and controls the width of that channel, which is defined by hydrophobic barriers. The resulting channel width ( $W_h$ ) and height ( $H_h$ ) are tunable according to the heating conditions used during thermal laminating.

One of the important fabrication parameters is the heating time at a fixed temperature because it determines the viscosity and spreading of the molten wax. We investigated the controllable range of heated height with several heating times by melting the wax patterns at a constant temperature for time intervals ranging from 0.06 to 0.44 sec. The influence of the heating time on the formation of the heated height was estimated by analyzing cross-sectioned images formed by the spread wax patterns (Fig. 2B). As expected, the heating time had a linear relationship with the square of the heated height and width but with different slopes. The linear relationship indicates that the printing and heating process is reproducible and predictable. Additionally, the cross-sectioned images showed the difference in the lateral and vertical spreading of wax. The results confirm that the lateral spreading of the printed wax is more extensive than vertical spreading, most likely because of the horizontal alignment of the fibers in the paper.<sup>23</sup> Thus, it seems possible to

design a 3D-microfluidic network using this simple fabrication method with channels of different predictable width and height simply by controlling the heating time.

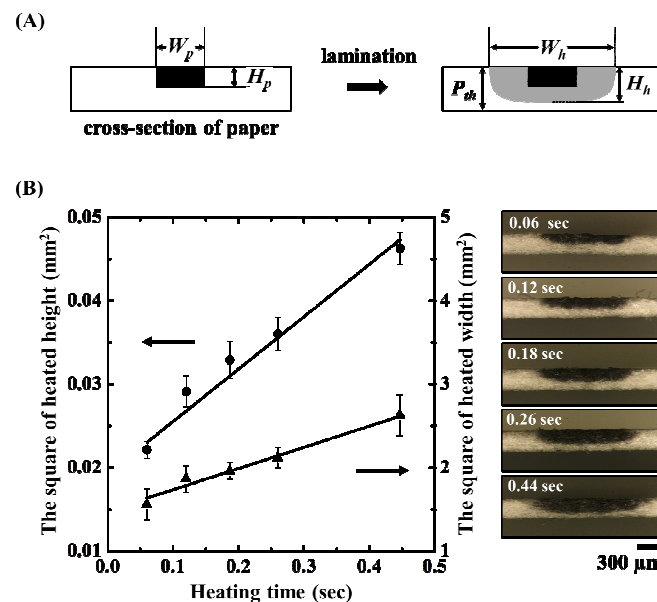


**Fig. 2** Changes in the heated height ( $H_h$ ) and heated width ( $W_h$ ) from the vertical and lateral spreading of the printed wax line ( $W_n = 1.0$  mm) as a function of heating time ( $t$ ). (A) Schematic illustration of the spreading process for molten wax in a cross-section of paper.  $W_p$  and  $H_p$ , respectively, are the width and height of the printed wax.  $W_h$  and  $H_h$ , respectively, are the width and height of the wax lamination. (B)  $H_h$  and  $W_h$  increase depending on the heating time, as well as the actual images of wax printed, after heating at 140 °C.

### The heated height as a function of nominal width

In case of double-sided wax printing onto a single sheet of paper, on a cross-section of the paper, the wax is divided into the front- and back-printed wax (Fig. S1).<sup>†</sup> First, we investigated the effect of the nominal width ( $W_n$ ) on the change in the heated height ( $H_{hf}$  and  $H_{hb}$ ) because controlling the heated height is crucial in designing a 3D- $\mu$ PAD. Fig. 3 shows the change in the heated height ( $H_h$ ) in accordance with different nominal widths ( $W_n$ ; 0.1 – 2.0 mm) and heating times (0.06 – 0.44 sec) at 140 °C. All of the experimental data show typical saturation curves, but with different linear ranges. Based on this result, we determined that the heated height ( $H_h$ ) is almost constant, regardless of heating time, when  $W_n$  is larger than 0.8 mm. This result provides a convenient design rule for creating channels in the paper because we can reliably fabricate channels with a predictable, fixed height if the nominal width is above 0.8 mm. Furthermore, this constancy of the heated height ( $H_{hf}$ ) is a useful characteristic for predicting whether a 3D-microfluidic network will be formed in a single sheet at specific heating time.

Next, we determined the fabrication conditions for the formation of a docking wax barrier with a minimum heating time and the smallest  $W_n$  required to produce fully functioning hydrophobic barriers in the paper. For this experiment, we designed a circular fluid reservoir that was separated from a concentric circular test zone by a hydrophobic barrier. Inner circles with a nominal width ranging from 0.2 – 1.8 mm and in 0.2 mm increments were printed into 2.0 mm outer circles

because printed circles are effectively a combination of vertical and horizontal lines (Fig. 3B, Fig. S3). A red food dye solution with a volume of 10  $\mu\text{L}$  was applied, which could fully fill the inner and outer circle. The smallest functional hydrophobic barrier (docking wax barrier) that prevented fluid from flowing out were obtained when 0.8 and 0.4 mm  $W_n$  were applied at 0.26 and 0.44 sec heating time, respectively.

Importantly, there was always a fluid leaking problem if the docking-wax-barrier was not formed at sufficient heating time (0.06 - 0.18 sec) (Fig. 3B). These results are consistent with the relationships shown in Fig. 3(A). As expected based on the results for wax spreading in the paper, docking wax barriers with nominal widths of  $> 0.8$  mm generated functional hydrophobic barriers in 100% of the experiments, regardless of the heating time.

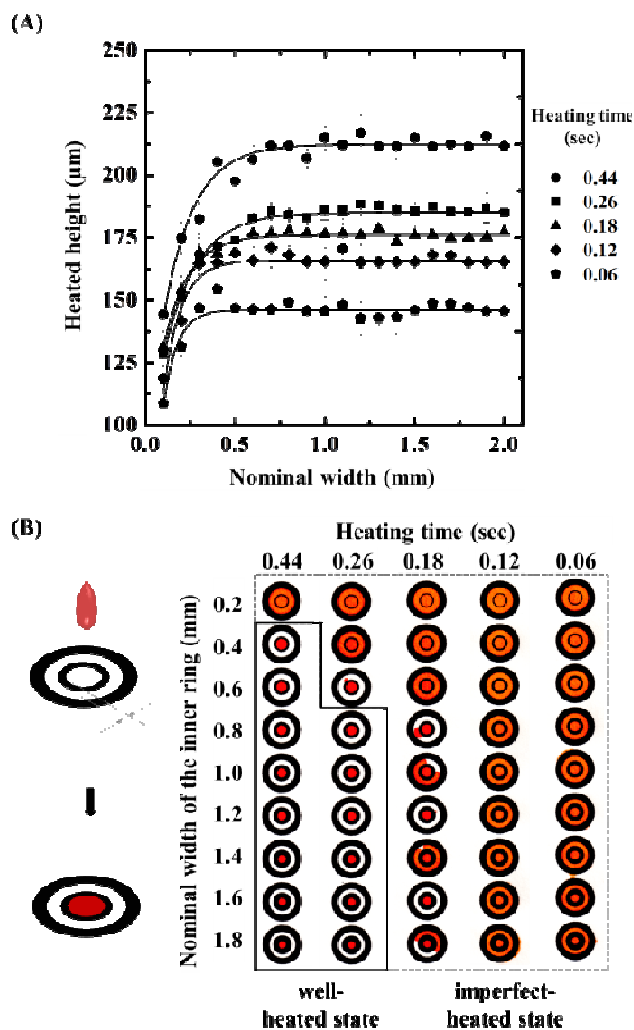


**Fig. 3** (a) The heated height of the front side of the sheet ( $H_{hp}$ ) as a function of the nominal width ( $W_n$ ) for various heating times, ranging from 0.06 to 0.44 sec, at 140  $^{\circ}\text{C}$ . (b) Optimum resolution of the printing condition for the formation of a docking wax barrier. The smallest functional circular barrier was determined by testing barriers with a range of nominal widths (0.2 – 1.8 mm) and various heating times (0.06 – 0.44 sec).

### 3D-microfluidic channel

We also demonstrated the ability of the microfluidic channel to move fluids in 3D-space. As expected, a cross-sectioned image showed that a docking wax hydrophobic barrier, an inlet, a lower-channel, an upper-channel, and an outlet were perfectly fabricated using the simple printing and thermal lamination method (Fig. 4A). When a red dye solution was loaded into the left inlet, the solution flowed horizontally and vertically from the inlet to the outlet through the fabricated 3D-microfluidic channel (Fig. 4B). The docking wax hydrophobic barrier prevented fluid from leaking and formed the inlet and outlet in the single sheet of paper.

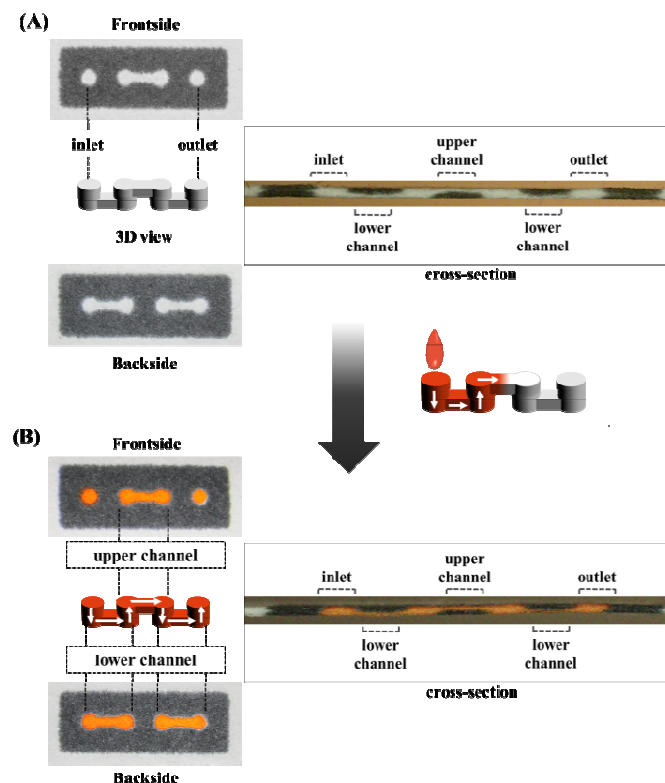


**Fig. 4** Demonstration of a 3D microfluidic network in a single sheet of paper. (A) Front and backside image of a sheet of paper after printing and heating for 0.26 sec at 140  $^{\circ}\text{C}$ . The cross-section image shows the formation of docking wax, an inlet, a lower-channel, an upper-channel, and an outlet in a single sheet of paper. (B) Front and backside images of a sheet of paper after loading a red dye solution into the inlet. The cross-section image indicates that red dye solution flows from the inlet to the outlet without leakage via the lower- and upper-channels alternatively.

The lower and upper channels guided the horizontal flow of fluid, while the interim between the lower and upper channels induced vertical fluid flow. Based on this basic design rule, we expanded this concept to demonstration the quantification of analytes in a 3D- $\mu\text{PAD}$  without using an external detection apparatus.<sup>25</sup>

### 3D- $\mu\text{PAD}$ for the diagnosis of albuminuria and glycosuria

Conventional methods for measuring output signals in point-of-care (POC) devices are accomplished by expensive external readers, such as hand-held electrochemical, absorbance,

reflectance, transmittance, or fluorescence devices, for precise quantitative detection.<sup>26-30</sup>

Here, we present complimentary assay strategy to surmount the “equipment-free” issue.<sup>4, 6, 12</sup> By using a 3D-microfluidic network in a single sheet of paper, where the direction of a three-dimensional fluid can be controlled, the level of an analyte can be measured simply by counting the number of reacting dots whose color changes in response to the amount of analyte in a sample solution. This approach involves a (bio)chemical reaction between analytes in a sample and a reagent in diagnostic dots the solution passes through in a single conduit within a 3D- $\mu$ PAD. The dots become blue-colored after loading a sample containing analyte. A representative design of a 3D- $\mu$ PAD (dimensions: 30 mm width, 33 mm length, 290  $\mu$ m thickness) containing a sample pad, BSA dots, and a glucose dot was formed by the simple double-sided printing and heating process on a single sheet of paper to create a single hydrophilic conduit that extends in the z-direction from the inlet to the outlet (Fig. 5 and Fig. S4).<sup>†</sup> This 3D- $\mu$ PAD distributes sample from a single sample pad on the device into BSA and glucose sensing dots. In this study, feasibility for the diagnosis of albuminuria and glycosuria was performed because albuminuria ( $> 0.3 \text{ mg mL}^{-1}$  in urine) can be a crucial sign that protein is leaking through the glomeruli in the kidney, while glycosuria is a symptom where a high concentration of glucose exists in urine ( $200 \text{ mg dL}^{-1}$ ) because it exceeds the kidney threshold.<sup>25</sup> This 3D- $\mu$ PAD based on selective changes in reagent color was fabricated because albumin was used as a model analyte. Albumin selectively reacted with TBPB that was deposited into defined regions of the hydrophilic microfluidic conduit prior to sample loading, whereas glucose (a model small chemical analyte) sequentially reacted with glucose oxidase and horseradish peroxidase that were adsorbed in a circle on the bottom region of the 3D- $\mu$ PAD (Fig. 5). As little as  $2 \mu\text{L}$  of sample could be added to the top of the sample loading dot, and the fluid was divided into two flows toward the BSA and glucose dots, respectively (Fig. 5A).

The color change in the albumin detecting dots appeared when the sample had flowed through the entire microfluidic conduit (Fig. 5B). Moving from left to right, the yellow colored TBPB reagent in the dots changed to blue via reaction with albumin, and the extent of the color change depended on the concentration of the sample solution. Flowing sample through the microfluidic conduit allowed for a consecutive color change as albumin molecules in the passing sample fluid are consumed by reaction with TBPB. Thus, we can easily measure the concentration of the sample by simply counting the number of colored dots. This assay provides a novel format for digital diagnostics to indicate the amount of BSA.

We examined the relationship between BSA concentration and the number of dots showing a color changed by introducing samples with various concentrations of BSA into the sample pad. Then, we counted the number of green dots. As expected, the increase in the number of green dots depended on the concentration of BSA in the sample (Fig. 5C, Fig. S6). Secondly, the sample also flowed from the sample pad to the glucose dot through another microfluidic conduit in the 3D- $\mu$ PAD. A mixture of glucose oxidase, horse radish peroxidase, and potassium iodide were absorbed in the glucose dot prior to sample loading, which resulted in the glucose dot having a brown color in the presence of glucose (Fig. 5 and Fig. S4).<sup>†</sup> When a sample with BSA ( $1.0 \text{ mg mL}^{-1}$ ) and glucose ( $50 \text{ mg mL}^{-1}$ ) was loaded, the 3D- $\mu$ PAD clearly indicated four blue colored dots and a red glucose dot. This result shows that the

3D- $\mu$ PAD can simultaneously perform multiple diagnostic assays under this novel format of digital diagnostics.

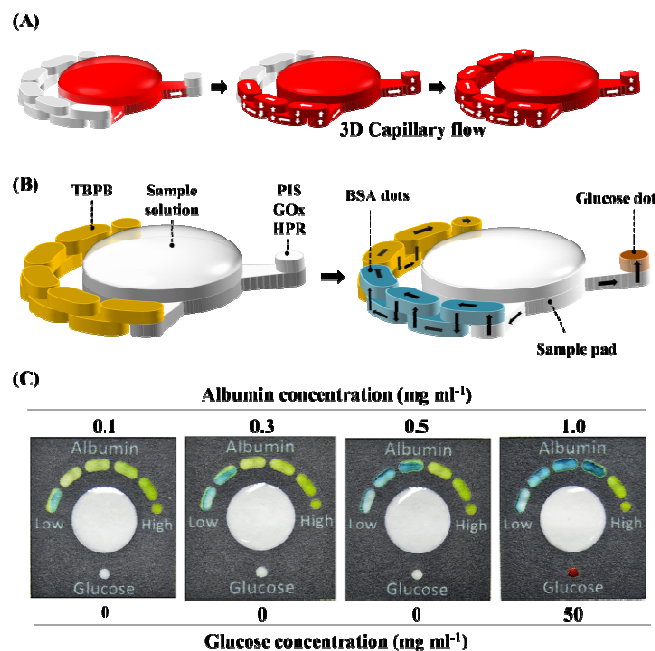


**Fig. 5** The 3D- $\mu$ PAD for a multiplexed and digital assay. BSA dots could quantify the level of BSA by simply counting the number of colored dots, while the glucose dot could detect the presence of glucose in a sample. (A) Illustration of three-dimensional flow in a device fabricated in a single sheet. Solution is absorbed into the sample pad and divided into the BSA and glucose dot. The sample solution flows from the first dot to the final dot through upper- and lower-channels, alternatively. (B) The microfluidic conduit of the BSA-dots in the 3D- $\mu$ PAD was functionalized by wicking with a mixture of tetrabromophenol blue (TBPB) and citrate buffer solution to enable the detection of BSA. In case of the glucose-dot, a mixture of potassium iodide (PI), glucose oxidase ( $\text{GO}_x$ ), and horseradish peroxidase (HPR) was wicked. After injecting a sample solution containing BSA and glucose, the green colored BSA-dots changed to blue in accordance with the amount of BSA. (C) Snapshot images of the digital assay after the introduction of a sample solution with different concentrations of BSA or glucose. The number of blue colored dots showed a linear relationship with the BSA concentration in the sample solution. The colorless glucose-dot also changed to a brown color when glucose was present.

## Conclusions

In conclusion, herein we demonstrated a simple fabrication method for forming a 3D-microfluidic network in a single sheet of paper. This rapid method can drastically reduce the production time for 3D- $\mu$ PAD and is applicable for digital assays that operate by counting the number of colored bars, without the need for an external analytical apparatus. These properties make these devices a useful platform for developing the types of diagnostic assays sought by the World Health Organization for use in the developing world.

Although this initial proof-of-concept study shows the feasibility for the detection of albumin and glucose as model analytes, we hope that this rapid process will contribute to the realization of a zero-cost diagnostic sensor as soon as possible and dramatically reduce diagnostic expenses for our aging society and developing countries by facilitating the development digital assays in paper microfluidics.

## Nomenclature

$W_n$	Nominal width (the width of the wax-pattern designed in the image software (Adobe illustrator CS6)).
$W_p$	Printed width (the width of the wax-pattern printed on paper).
$W_h$	Heated width (the width of the heated-wax pattern after melting the printed-wax pattern).
$H_p$	Printed height (the height of the printed-wax pattern on the cross-section of the paper).
$H_{pf}$	Printed height on the front side of the sheet.
$H_{pb}$	Printed height on the backside of the sheet.
$H_h$	The heated height (the height of the resulting heated-wax pattern on the cross-section of paper after melting the printed-wax pattern).
$H_{hf}$	$H_h$ of the front-side sheet (the height of an upper-heated-wax pattern).
$H_{hb}$	$H_h$ of the back-side sheet (the height of a lower-heated-wax pattern).
$P_{th}$	The thickness of the paper after lamination.
$H_{UC}$	The height of an upper-channel.
$H_{LC}$	The height of a lower-channel.

## Acknowledgements

This research was supported by the Basic Science Research Program through the National Research Foundation of Korea (NRF) funded by the Ministry of Science, ICT & Future Planning (MSIP) (No. NRF-2011-0017322)

## Notes

<sup>a</sup> Department of Chemical Engineering, Chungnam National University, Yuseong-gu, Daejeon 305-764, Republic of Korea. E-mail: rhadam@cnu.ac.kr; Tel: +82-42-821-5896.

<sup>b</sup> Micro/Nano Scale Manufacturing Research Group, Korea Institute of Industrial Technology, Ansan-si, Gyeonggi-do, 426-910, Republic of Korea.

† Electronic Supplementary Information (ESI) available: See DOI: 10.1039/b000000x/

## References

- D. E. Bloom, D. Canning and G. Fink, *Oxford Review of Economic Policy*, 2010, **26**, 583-612.
- W. J. Spitzer and K. W. Davidson, *Soc Work Health Care*, 2013, **52**, 959-986.
- P. von Lode, *Clinical biochemistry*, 2005, **38**, 591-606.
- R. W. Peeling, K. K. Holmes, D. Mabey and A. Ronald, *Sexually transmitted infections*, 2006, **82**, v1-6.
- A. W. Martinez, S. T. Phillips, M. J. Butte and G. M. Whitesides, *Angewandte Chemie*, 2007, **46**, 1318-1320.
- G. G. Lewis, M. J. DiTucci and S. T. Phillips, *Angewandte Chemie*, 2012, **51**, 12707-12710.
- A. K. Yetisen, M. S. Akram and C. R. Lowe, *Lab Chip*, 2013, **13**, 2210-2251.
- C. Parolo and A. Merkoci, *Chemical Society reviews*, 2013, **42**, 450-457.

- S. G. Jeong, J. Kim, J. O. Nam, Y. S. Song and C. S. Lee, *International neurology journal*, 2013, **17**, 155-161.
- R. V. Taudte, A. Beavis, L. Wilson-Wilde, C. Roux, P. Doble and L. Blanes, *Lab Chip*, 2013, **13**, 4164-4172.
- S. G. Jeong, S. H. Lee and C. S. Lee, *KSBB Journal*, 2013, **28**, 254-259.
- D. M. Cate, W. Dungchai, J. C. Cunningham, J. Volckens and C. S. Henry, *Lab Chip*, 2013, **13**, 2397-2404.
- G. E. Fridley, H. Le and P. Yager, *Analytical chemistry*, 2014.
- A. W. Martinez, S. T. Phillips, Z. Nie, C. M. Cheng, E. Carrilho, B. J. Wiley and G. M. Whitesides, *Lab Chip*, 2010, **10**, 2499-2504.
- Y. K. Oh, H. A. Joung, S. Kim and M. G. Kim, *Lab Chip*, 2013, **13**, 768-772.
- A. W. Martinez, S. T. Phillips and G. M. Whitesides, *Proceedings of the National Academy of Sciences of the United States of America*, 2008, **105**, 19606-19611.
- G. G. Lewis, M. J. DiTucci, M. S. Baker and S. T. Phillips, *Lab Chip*, 2012, **12**, 2630-2633.
- L. Ge, S. Wang, X. Song, S. Ge and J. Yu, *Lab Chip*, 2012, **12**, 3150-3158.
- J. D. Peele, Jr., R. H. Gadsden and R. Crews, *Clinical chemistry*, 1977, **23**, 2242-2246.
- A. Rad, M. Jahanshahi, M. Ardjmand and A.-A. Safekordi, *Korean J. Chem. Eng.*, 2012, **29**, 1766-1770.
- M. J. Puglia, J. A. Lott, J. A. Profitt and T. K. Cast, *Journal of clinical laboratory analysis*, 1999, **13**, 180-187.
- Y. J. Wei, K. A. Li and S. Y. Tong, *Talanta*, 1996, **43**, 1-10.
- E. Carrilho, A. W. Martinez and G. M. Whitesides, *Analytical chemistry*, 2009, **81**, 7091-7095.
- E. W. Washburn, *Phys. Rev.*, 1921, **17**, 273.
- W. H. O. and I. D. F. Consultation, *Definition and diagnosis of diabetes mellitus and intermediate hyperglycaemia*, World Health Organization, Switzerland, 2006.
- W. Dungchai, O. Chailapakul and C. S. Henry, *Analytical chemistry*, 2009, **81**, 5821-5826.
- C. M. Cheng, A. W. Martinez, J. Gong, C. R. Mace, S. T. Phillips, E. Carrilho, K. A. Mirica and G. M. Whitesides, *Angewandte Chemie*, 2010, **49**, 4771-4774.
- A. W. Martinez, S. T. Phillips, E. Carrilho, S. W. Thomas, 3rd, H. Sindi and G. M. Whitesides, *Analytical chemistry*, 2008, **80**, 3699-3707.
- A. K. Ellerbee, S. T. Phillips, A. C. Siegel, K. A. Mirica, A. W. Martinez, P. Striehl, N. Jain, M. Prentiss and G. M. Whitesides, *Analytical chemistry*, 2009, **81**, 8447-8452.
- N. K. Thom, K. Yeung, M. B. Pillion and S. T. Phillips, *Lab Chip*, 2012, **12**, 1768-1770.